Liquid Crystals
Publication details, including instructions for authors and subscription information:
http://www.informaworld.com/smpp/title~content=t713926090

Smectic ordering in side-chain liquid crystalline polymers (LCPs) and in LCP-silica nanocomposites

Fabiano Vargas Pereira[a]; Aloir Antonio Merlo[b]; Françoise Bley[c]; Isabelle Morfin[d]; Olga Maria Ritter[b]; Nádya Pesce da Silveira[b]; Françoise Ehrburger-Dolle[d]
[a] Universidade do Estado da Bahia, Rua Silveira Martins, Bahia CEP: 41.195-001, Brasil [b] Universidade Federal do Rio Grande do Sul, Instituto de Química, CEP 91501 970 Caixa Postal 15003, Brasil [c] Science et Ingénierie des Matériaux et Procédés, UMR5266 CNRS- INPG-UJF, 38402 Saint-Martin d'Hères, France [d] Laboratoire de Spectrométrie Physique, UMR 5588 CNRS-UJF, 38402 Saint-Martin d'Hères, France

To cite this Article Pereira, Fabiano Vargas , Merlo, Aloir Antonio , Bley, Françoise , Morfin, Isabelle , Ritter, Olga Maria , da Silveira, Nádya Pesce and Ehrburger-Dolle, Françoise(2008) 'Smectic ordering in side-chain liquid crystalline polymers (LCPs) and in LCP-silica nanocomposites', Liquid Crystals, 35: 3, 299 — 313
To link to this Article: DOI: 10.1080/02678290701858338
URL: http://dx.doi.org/10.1080/02678290701858338

Liquid Crystals,
Vol. 35, No. 3, March 2008, 299–313

Taylor & Francis
Taylor & Francis Group

Smectic ordering in side-chain liquid crystalline polymers (LCPs) and in LCP–silica nanocomposites

Fabiano Vargas Pereira[a]*, Aloir Antonio Merlo[b], Françoise Bley[c], Isabelle Morfin[d], Olga Maria Ritter[b], Nádya Pesce da Silveira[b] and Françoise Ehrburger-Dolle[d]

[a]*Universidade do Estado da Bahia, Rua Silveira Martins, 2555 Salvador, Bahia CEP: 41.195-001, Brasil;* [b]*Universidade Federal do Rio Grande do Sul, Instituto de Química, Av. Bento Gonçalves 9500 Porto Alegre – Rio Grande do Sul, CEP 91501 970 Caixa Postal 15003, Brasil;* [c]*Science et Ingénierie des Matériaux et Procédés, UMR5266 CNRS- INPG-UJF, 38402 Saint-Martin d'Hères, France;* [d]*Laboratoire de Spectrométrie Physique, UMR 5588 CNRS-UJF, 38402 Saint-Martin d'Hères, France*

(Received 24 July 2007; final form 11 December 2007)

The mesophase behaviour of a side-chain liquid crystalline polyacrylate (LCP) grown by drying a solution has been investigated. This LCP, characterised by a short spacer (four carbon atoms) and a long tail (10 carbon atoms), displays, at increasing temperatures, SmC and SmA_d phases. The effect of the mean molecular weight, i.e. the mean number of side chains per polyacrylate main chain (18 and 51) on the lamellar width, was studied. LCP–silica nanocomposites have been synthesised by a sol-gel process in the presence of LCP in the solution, followed by subcritical drying. The mesophase behaviour of these nanocomposites was compared to that of the corresponding bulk LCP. The experimental methods were polarised optical microscopy, differential scanning calorimetry and synchrotron X-ray scattering.

Keywords: side-chain liquid crystal polymer; silica xerogel; LCP–silica nanocomposites; SAXS

1. Introduction

Liquid crystalline polymers (LCPs) combine liquid crystal (LC) anisotropic ordering and specific polymer properties (*1*). Therefore, they have been widely investigated over the last two decades (*2–8*). Among them, side-chain liquid crystalline polymers (SCLCP) have attracted a great deal of interest because these materials display a rich variety of mesophases (*9, 10*). These characteristics make them suitable not only for applications in displays, in optical data storage or in non-linear optics (*11–13*) but also in chromatography, as separation membranes, as solid polymer electrolytes and now as structural materials (*13*). The properties of the LC state are firstly related to the nature of the main polymeric chain (or backbone) (*14*). For a given backbone, the mesophases depend mainly on three parameters: the length of the spacer (*15, 16*) that links the mesogenic group to the main chain (polymeric backbone), the nature of the mesogenic group (*1, 2, 17*) and, if any, the length and chemical nature of the terminal tail (*18*) as well as the degree of polymerisation of the main chain (*19*). The large number of parameters would eventually allow tailoring of LCPs for a given required mesophase structure, if structure–property relationships are known. To this end, a series of new liquid crystalline polyacrylates have recently been synthesised and characterised (*20–22*).

Nowadays, the demand of nanotechnology opens a new field of investigation: LCP-organic or -inorganic nanocomposites. A few years ago, Vaia and Giannelis (*23*) described a direct intercalation of thermotropic LCP into layered silicates. Huang and Han (*24, 25*) have shown the possibility of designing thermotropic LCPs that can give rise to highly dispersed organoclay aggregates in nanocomposites without sacrificing the liquid crystallinity of the LCP. Also, main chain type thermotropic LC polyimides–silica nanocomposites were obtained by a sol-gel reaction performed in a solution containing the precursor of LC polyimide (*26*). LCP nanocomposites raise also the question of the effect of confinement on the liquid crystalline properties of LCPs. Confinement of liquid crystals in organic or inorganic matrices has been widely investigated for low molecular weight LC, such as 8CB (*27, 28*). We have recently investigated the effect of confinement into a silica aerogel on the LC ordering of side-chain LC polyacrylates (*29*). We have shown that the smectic layering is retained and that the smectic domain is shifted to lower temperatures in the confined LCP.

The aim of the paper is twofold. It is first to investigate the effect of the polymer molecular weight on the polymorphism of a side-chain LC polyacrylate characterised by a short spacer and a long terminal tail. The second goal is to investigate the effect of

*Corresponding author. Email: fvpereira@uneb.br

ISSN 0267-8292 print/ISSN 1366-5855 online

DOI: 10.1080/02678290701858338
http://www.informaworld.com

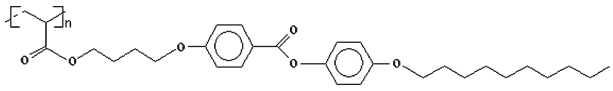

Figure 1. Chemical structure of the side-chain LC polyacrylate.

confinement into a silica matrix and to compare the results with that obtained for the bulk LCP. In contrast with the previous paper (*29*), the LCP–silica nanocomposite was prepared by a sol-gel reaction in the presence of LCP in the solution. The thermotropic behaviour of the bulk SCLC was probed by differential scanning calorimetry (DSC) and polarised optical microscopy (POM). X-ray scattering measurements, using synchrotron radiation, were performed in order to allow the mesophase characterisation and to investigate the local packing of the mesogenic units and the polymer backbone in bulk and confined in the silica xerogels for two different LCP molecular weights. The present investigation considers samples that have not been heated before, i.e. for which crystallisation was achieved in solution, during drying of the solvent. The comparison with samples crystallised from the melt (above the isotropic temperature), either for ordering in a magnetic field or for impregnation in silica aerogels, will be presented in a forthcoming paper.

2. Experimental section

2.1. *Materials*

The LCPs were synthesised using direct radical polymerisation of a mesogenic metacrylate monomer according to the procedure described elsewhere (*20*). Figure 1 shows the general chemical structure of the LC polyacrylate studied in this work. This polyacrylate has a spacer containing four methylene carbons and 10 alkyl carbons in the terminal tails. The two samples (LCP2 and LCP4) differ by their degree of polymerisation, P_w, and, therefore, by the number of side chains, which are equal to 18 and 51 for LCP2 and LCP4, respectively (Table 1). The molecular weights are relative to polystyrene standards and they have been characterised using a Waters 150C GPC system.

Confinement in silica xerogels was achieved by performing the sol-gel reaction in the presence of LCP in solution. The silica precursor was prepolymerised tetraethoxysilane (TEOS), named P750, and commercially available from the French Company PCAS. Details of silica gel preparations are given in (*30*). In the present case, the sol-gel reaction was performed using NH_4OH as catalyst and THF as solvent in which the present LCPs are soluble. The amounts of P750 (0.5 g), THF (0.5 g), NH_4OH (0.005 g) and LCP (0.018 g) were the same for both LCP2 and LCP4. After gelation (about 1 hour), the gels were dried in subcritical conditions at room temperature, yielding LCP–silica nanocomposites named LCP2–xero and LCP4–xero, respectively.

2.2. *Methods of characterisation*

POM was performed with an Olympus BX41 polarising microscope equipped with a Leitz Wetzlar 417 heating stage. Micrographs were obtained using non-treated glass slides. POM allowed the observation of the LC texture as well as the determination of the phase transition temperature of bulk LCPs. LCP–silica nanocomposites were too opaque to be investigated by this optical method.

DSC measurements were made on bulk samples of LCP2 and LCP4 by means of a Perkin Elmer DSC4. The rate of heating was 10°C/min.

SAXS experiments were performed at the European Synchrotron Radiation Facility (ESRF)[a], Grenoble, France on the French CRG beamline D2AM. The beam optics was adjusted to a narrow spot in order to avoid a broad incident X-ray beam. In the present case, the X-ray wavelength λ was equal to 1 Å (energy = 12.4 keV). In such conditions, the mean width of the X-ray beam on the detector was less than 3 pixels. Samples were placed in stainless steel sample holders closed by two mica windows mounted on a thermostatically controlled sample changer. As for DSC measurements, the samples have not been heated before the experiment. SAXS measurements were performed at stepwise

Table 1. Influence of the characteristics of the polymer chain on the phase behaviour of LCPs.

	$\overline{M}_w$	$\overline{M}_n$	$\overline{M}_w/\overline{M}_n$	P_w	K	T (°C)	SmC	T (°C)	SmA	T (°C)	I
LCP2	13,531	9200	1.47	18	•	47	•	120	•	172	•
LCP4	34,482	25,600	1.35	51	•	50	•	144	•	176	•

$\overline{M}_w$ and $\overline{M}_n$ are the weight average and the number average molar mass, respectively. The polydispersity is given by $\overline{M}_w/\overline{M}_n$ and the degree of polymerisation is defined as $P_w = \overline{M}_w/M_0$ where M_0 is the monomer mass. As a first approximation, P_w is close to n, the number of side chain per backbone chain. The phase transition temperatures are deduced from POM images.

[a]http://www.esrf.eu/

increasing temperatures, ranging from room temperature to 185°C. At each step, a waiting time of 10 min allowed temperature stabilisation. The indirect illumination CCD detector (Princeton Instruments) was located 80.5 cm from the sample. Data obtained from the detector were corrected by taking into account the flat field and the dark current. The images were processed by means of the software *bm2img* available on the beamline[b]. For anisotropic patterns the detector area was divided into 32 angular sectors and azimuthal averaging was performed in each 11.25° sector. Calibration of the *q*-scale was obtained by means of silver behenate (*31*). Finally, the data were corrected to allow for sample transmission and background scattering using an empty cell as reference.

3. Results and discussion

3.1. *Polarised optical microscopy*

Figure 2 shows typical SmC and SmA textures obtained using POM for both polyacrylates.

Figure 2(a) shows a Schlieren SmC phase with homeotropic alignment (75°C) for LCP2. In this alignment the phase director is orthogonal to the layer planes whereas in the homogeneous alignment the director is parallel to the substrate. Figure 2(b) shows a SmA fan-texture for the same polymer, with the appearance of black regions, characterising the melt of the LCP (isotropic phase). Figure 2(c) shows the SmC texture obtained for LCP4 polymer at 120°C and Figure 2(d) shows the SmA fan-texture obtained at 150°C. The texture shown in Figure 2(c) corresponds to a broken fan-shaped texture, with the appearance of equidistant lines on the surface of the fan. These features are characteristic of the SmC mesophase in the homogeneous alignment (*32*). In Table 1 the mesophases that could be characterised using the POM technique are shown. It appears that the K-SmC and the SmA-I transition temperatures decrease slightly when the molecular weight is smaller while the decrease of the SmC–SmA transition temperature is much larger.

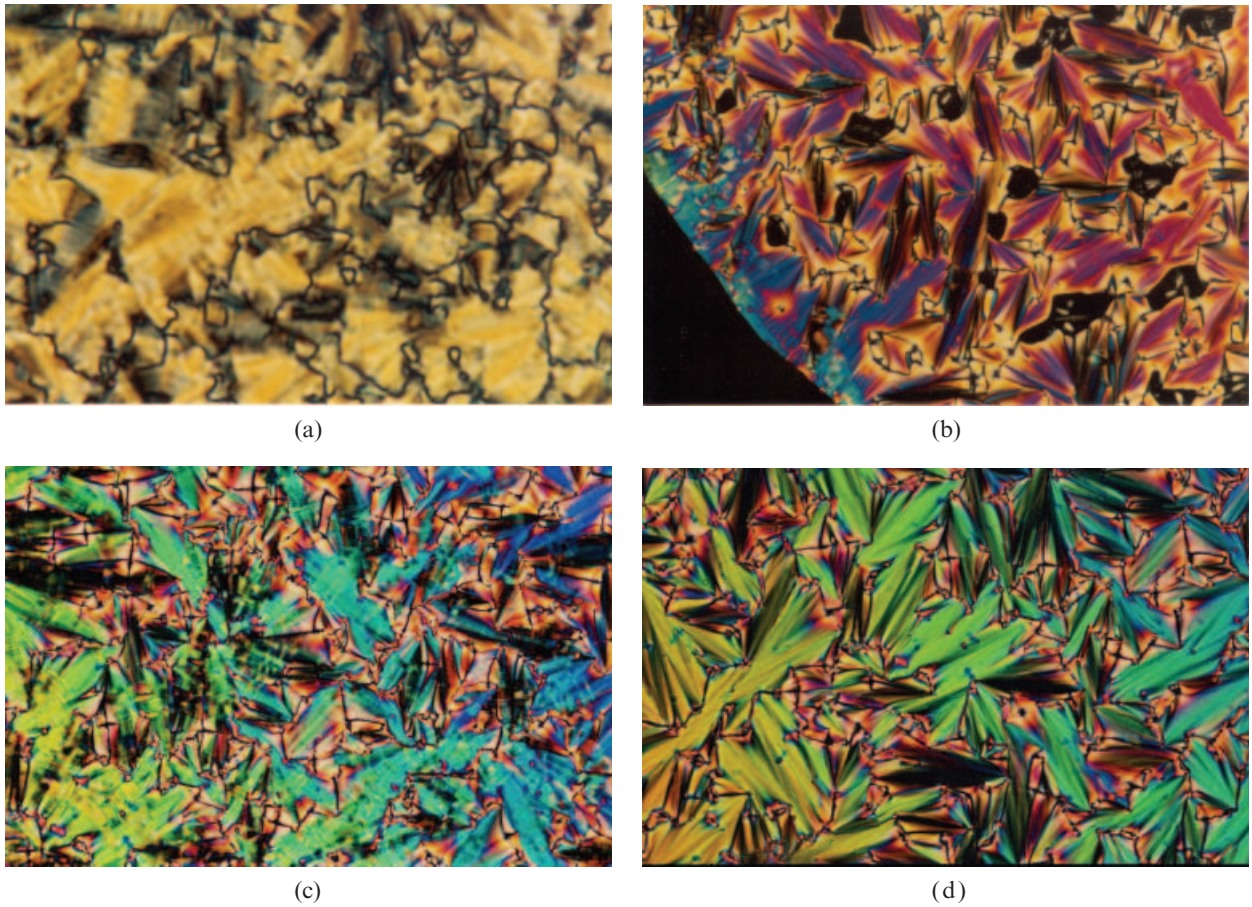

Figure 2. Optical micrographs of LCP2: (a) Schlieren SmC mesophase at 75°C; (b) coexisting SmA and isotropic phases at 168°C. Optical micrographs of LCP4: (c) SmC at 120°C; (d) SmA at 150°C.

[b]http://www.esrf.fr/exp_facilities/BM2/BM2.html

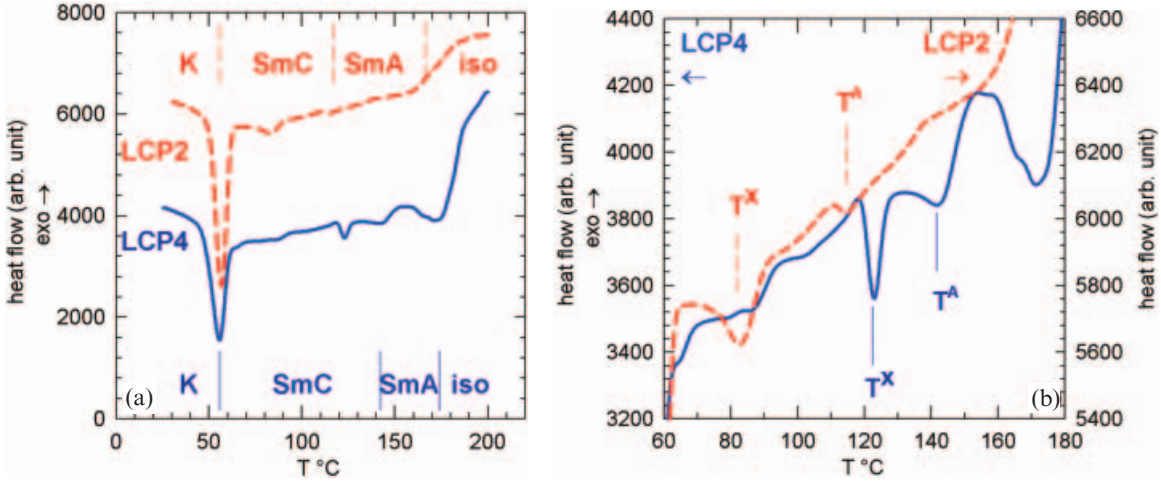

Figure 3. DSC heating curves (first heating) obtained for bulk LCP2 and LCP4 (a); (b) is an enlargement of (a).

3.2. *DSC curves*

DSC curves for both polymers are plotted in Figure 3. The first endothermic peak (T_m=55°C) is related to the solid crystal to LC transition. The last thermal event (around 170°C) corresponds to the isotropisation temperature T_I, in agreement with the above POM results. Figure 3(b) shows, for both samples, the existence of two endothermic peaks, T^X and T^A, between these two temperatures. The peak intensity as well as the peak temperature are smaller for LCP2 (T^X=83°C, T^A=114°C) than for LCP4 (T^X=123°C, T^A=142°C). From POM experiments, it may be concluded that T^A corresponds to a SmC–SmA transition. The presence of an endothermic peak located between the crystal to smectic transition temperature and the SmC to SmA transition was also reported by Watanabe et al. (*33*). The origin of the thermal effect yielding a peak at T^X will be discussed simultaneously with the SAXS results in section 3.5. The shape of the peak T^A suggests that the SmC–SmA transition is a first order one, similarly to what is observed for SmC*–SmA (ferroelectric LC) (*34, 35*), yet LCP2 and LCP4 are not ferroelectric. Such a debate (*36*), however, goes beyond the scope of the present paper.

3.3. *Evolution of the SAXS curves as a function of temperature*

Figures 4(a)–(d) show the temperature dependence of the scattering profiles obtained at raising temperatures for LCP2 and LCP4 in bulk and confined in a silica xerogel. For the sake of clarity, the curves have been shifted along the vertical axis. Each curve displays two peaks located at q_p and $2q_p$. This feature reveals the smectic ordering of the LCPs. At 165°C for LCP2 and 180°C for LCP4, the curves consist of a broad peak resulting from the liquid order of the polymer in the isotropic phase. Also all curves show that the position q_p of the peaks shifts to smaller q-values when the temperature increases up to a temperature T* that depends on the sample. Above T*, the position of the peaks starts to shift to greater q-values.

The comparison between the SAXS curves obtained for LCP2 (Figure 4(a)) and LCP4 (Figure 4(b)) allows significant differences to be mentioned. For LCP2, the curves measured below T* (≅140°C) clearly show that the peaks consist of several components. The SAXS pattern (the insert in Figure 4(a)) measured at 115°C indicates that scattering is nearly isotropic. Above T*, as for LCP4, only single peaks are observed over the whole range of temperature. Furthermore, for the latter the scattering is slightly anisotropic (I_{max}/I_{min}≅2) as shown by the azimuthal plot (Figure 5), measured at 155°C. Plots shown in figure 4 were all obtained by averaging the intensity over 360°. It can be shown that this procedure does not greatly modify the shape of the curves but it enlarges artificially the peaks. Therefore, fitting of the peaks presented in the next paragraph is made on data obtained by averaging intensity in sectors (11.25°).

The SAXS patterns obtained for LCP–xerogels (the inserts in Figures 4(c) and (d)) show a significant increase of the scattered intensity at small q-values, which results from scattering of the silica in the LCP–xerogel nanocomposites. The SAXS curves indicate that liquid crystalline ordering is still present at 185°C (the maximum temperature reached by the experimental device) for both LCP2 and LCP4–xerogel nanocomposites. This feature suggests that, for these

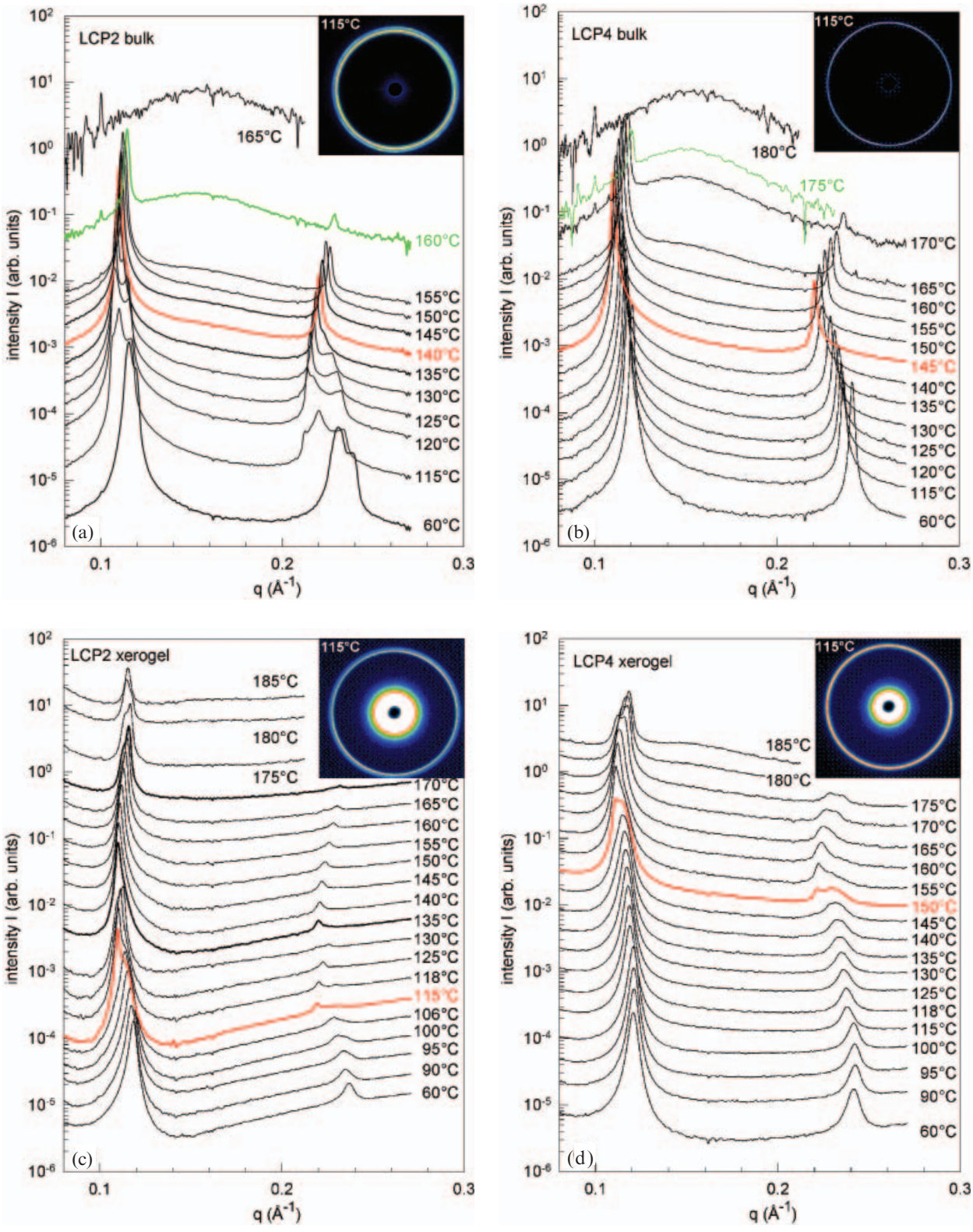

Figure 4. Temperature dependence of SAXS profiles of bulk LCP2 (a), bulk LCP4 (b), LCP2–xerogel (c) and LCP4–xerogel (d). The SAXS patterns (q-range 0.015 to about 0.16 Å^{-1}) viewed by the CCD camera are shown in the inserts: for bulk LCP2 (a) the pattern displays a nearly isotropic wide ring; for bulk LCP4 (b) a slight anisotropy can be detected (see also Figure 5); in the case of LCP–silica nanocomposite ((c) and (d)), the white region around the beamstop (low-q scattering) reveals a strong scattering coming from the porous silica matrix.

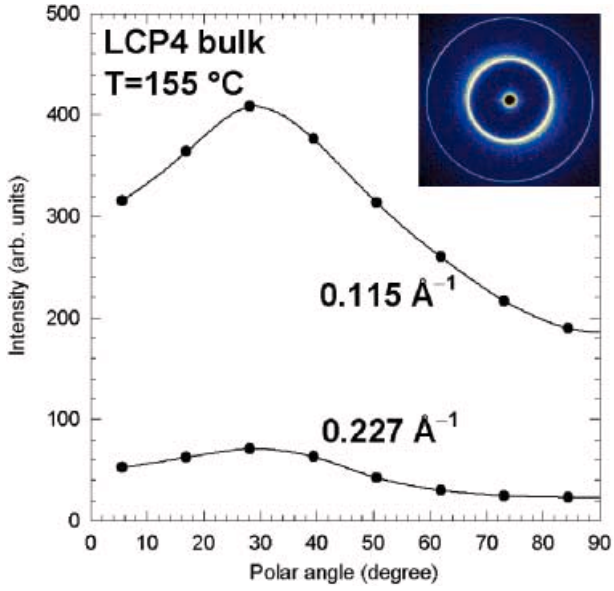

Figure 5. Azimuthal plots for bulk LCP4 at 155°C. The insert shows the corresponding SAXS pattern; the plot results from the analysis of the right lower quadrant.

systems, confinement increases the smectic to isotropic transition temperature whereas the opposite was observed for LC polyacrylates having a long spacer and a short tail confined in silica aerogels (*29*). The drawback is that it was not possible (*29, 37*) to determine the porous structure of the silica generally measured above the isotropisation temperature in the featureless polymer.

For LCP2, confinement in silica xerogel yields a reduction of the width (and the number of substructures) of the peaks. In contrast, LCP4 confined in silica xerogel exhibits a splitting into two peaks above 150°C.

Figure 6 shows the same curves as Figure 4 but plotted without vertical shift. The striking feature is the appearance of iso-intensity (or isosbestic) points P*. These points disappear for the bulk samples above 150°C and 160°C for LCP2 and LCP4, respectively. POM measurements indicate that vanishing of P* points coincides with appearance of black spots in the optical micrographs (as observed in Figure 2(b)), i.e. when the LC structure begins to melt (isotropic phase). Isosbestic points were reported by Dewettink et al. (*38*) during the last period of isothermal crystallisation of cocoa butter, suggesting that the phase change occurs without a modification of the total volume of the two phases. In the present case, one is probably dealing with a balance between diffraction of the ordered lamellar structure of the polymer and a polymer background scattering that could be due to the arrangement of backbone and/or long alkyl tails of the side chains. This question will be discussed further in the next section.

3.4. *Fitting of the first-order peaks*

A quantitative description of the X-ray scattering spectra of smectic LCs can be made by models developed for lyotropic lamellar phases (*39*); several functional forms have been proposed for confined low molecular weight LCs (*37, 40*) or confined LCPs (*29*). Figure 7 shows the SAXS data obtained for LCP4 at 145°C. The dashed line results from a fit of the experimental data by using a structure factor $S(q)$ and a form factor $P(q)$ given respectively by equation (14) and (19bis) in (*39*), subsequently named the NLR equation. The relevant fitting parameter η, related to the layer displacement fluctuations (thermal effect), and thus to the elastic constants of the smectic phase, is equal to 0.05. Nallet et al. have shown (Figure 6 in (*39*)) that thermal fluctuations yield a decrease of the ratio of the first harmonic to the fundamental peak intensities, I_2/I_1 from 1 (for $T=0$ K, $\eta=0$) to values smaller than 1. For $T>0$, the higher-order Bragg peaks are smoothed out. For lyotropic lamellar phases with an inter-lamellar distance d close to 60 Å, typical values of η range between 0.1 and 0.2. The smaller η value obtained for LCP4 at 145°C, which has a comparable interlayer distance as will be shown below, indicates that the layers are quite rigid. Figure 7 shows that the NLR equation yields a good estimation of the position and the relative intensity of the peaks but a very poor fit to the peaks, which are narrower than expected from the model. Among the possible explanations for this discrepancy one may suggest the fact that LCP4 is partly oriented, as shown in Figure 5. The fitting procedure was applied to peaks obtained by averaging the intensity over an azimuthal angle $\Delta\phi=12.25^{\circ}$. Therefore, the SAXS curve is not a true powder diagram as required for use of the NLR equation. Further work is required in order to find a model for these samples. In fact, this investigation goes beyond the scope of the present investigation that aims to analyse the variation of the interlayer distance as a function of the temperature and to separate the different peaks, particularly in the case of confined LCPs. Eventually, the variation of I_2/I_1 with temperature may give a trend of the evolution of the smectic layer rigidity during heating.

For all the above reasons, the peaks were fitted with a pseudo-Voigt equation,

$$f_1(q)=I_1\left[a_1\frac{1}{1+(q-q_1)^2\xi_1^2}+(1-a_1)\exp\left[-0.5(q-q_1)^2\xi_1^2\right]\right] \quad (1)$$

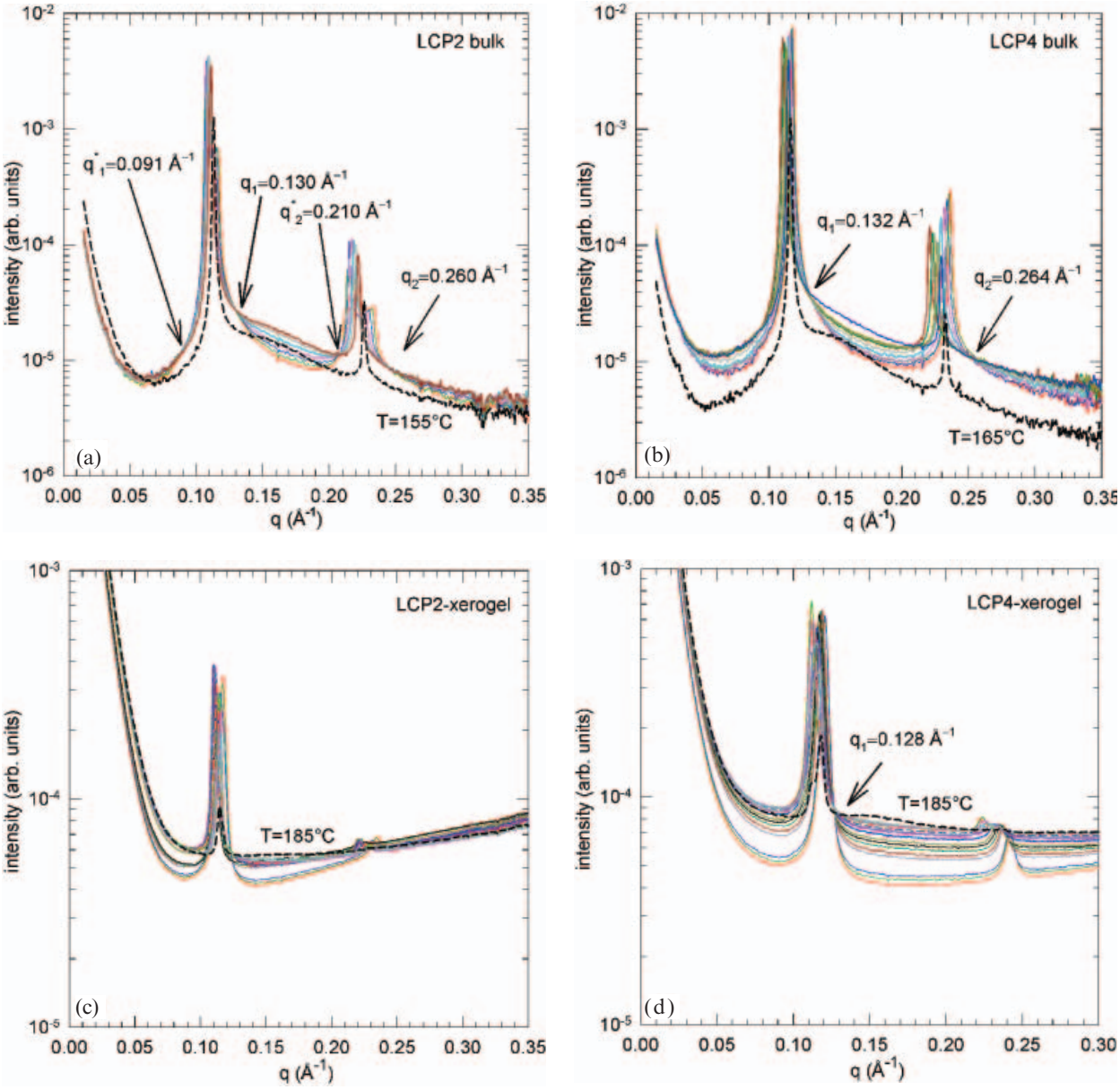

Figure 6. Same plots as in Figure 4 without vertical shift. The iso-intensity points are indicated by arrows. The curves correspond to temperatures varying: for LCP2 (a), between 115 and 155°C; for LCP4 (b), between 115 and 165°C; for LCP–xerogel ((c) and (d)), between 90 and 185°C.

or a sum of pseudo-Voigt equations,

$$f(q) = \sum f_i(q), \tag{2}$$

in the case of peak splitting. The regression procedure was achieved by means of the Marquart–Levenberg algorithm in SigmaPlot® 8.02, SPSS. The resulting curve (the continuous line in Figure 7) does not fit well the low intensity wings. However, as shown for the curve plotted in linear coordinates (the insert in Figure 7), the fitting equation describes quite satisfactorily more than 90% of the peak intensity.

Examples of fits of peaks measured for bulk LCPs and LCP–silica xerogel nanocomposites are shown in Figures 8 and 9, respectively. For all bulk LCPs, the fitting procedure was applied to peaks obtained by averaging the intensity over an azimuthal angle $\Delta\phi = 12.25°$. The values of the fitting parameters, except for the maximum intensity I_1, do not change significantly from one sector to the other. For LCP–xerogel nanocomposites, no anisotropy is observed and thus fitting was performed on peaks obtained by radial averaging over 360°. Figure 8(a) shows the result of the fit by equation (1) for the fundamental

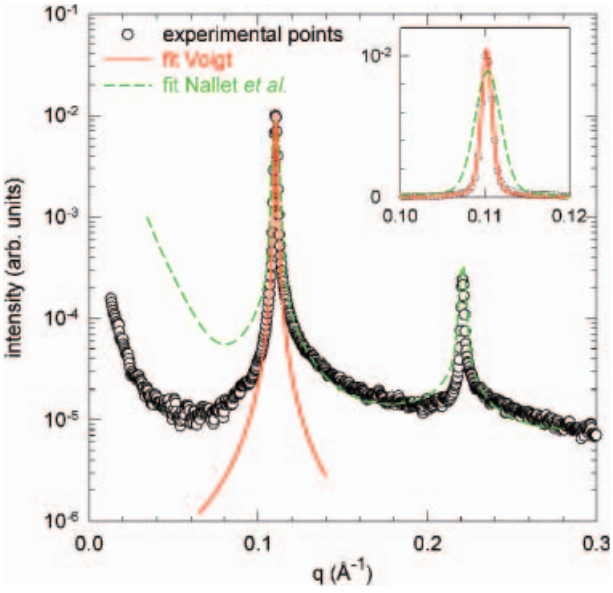

Figure 7. Fit of the SAXS curve obtained for LCP4 (145°C) by the equation proposed by Nallet *et al.* (*38*). The continuous line corresponds to the fit of the fundamental peak by a pseudo-Voigt equation (1). The fundamental peak is plotted in linear coordinates in the insert.

peak of LCP4 bulk measured at 115°C. The pseudo-Voigt equation was chosen owing to the impossibility of fitting any peak with a single Lorentzian or Gaussian equation (*19*) or by a sum of two Lorentzians as in the case of a low molecular weight LC (8CB) confined in silica aerogels (*37*). Meanwhile, in some cases, the pseudo-Voigt equation yields pure Gaussian or Lorentzian fits, e.g. for LCP2 (Figure 8(e)). The fraction a_1 of the Lorentzian contribution is smaller (a_1=0.42) for LCP4 heated at 155°C (Figure 8(b)) than it is for the sample heated at 115°C (a_1=0.71). The analysis of all the peaks obtained for bulk and confined LCPs suggests that below T^* (corresponding to the smallest q-value for the peak position) a_1 is close to 0.4–0.5 and becomes close to 0.7 above T^*.

In order to compare the measured intensity to that expected from the fitting curve near the wings, the data are plotted in a logarithmic scale (see the inserts in Figures 8(a), (b), (e) and (f)). In all cases, far from the peak centre, the experimental points are located above the fitting line, particularly on the high-q side of the peak. This observation suggests the occurrence of a q- and T-dependent background

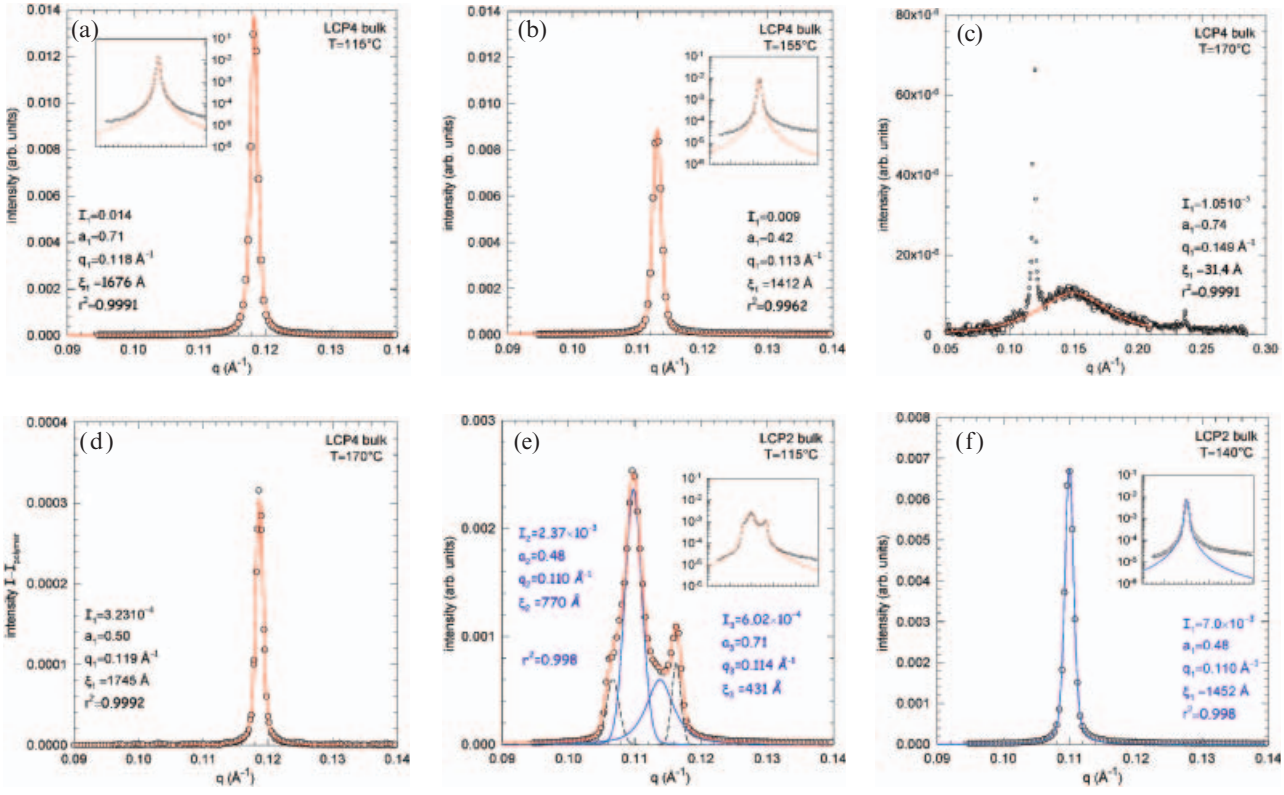

Figure 8. Examples of peak fitting in the case of bulk LCPs. In the inserts, the q-scale is the same as in the main frame and the intensity axis has a logarithmic scale. In (c), the fit of the polymer background is obtained after suppression of the data corresponding to the peak. In (d), the fit of the peak is performed after subtraction of the polymer background shown in (c). The curve obtained for LCP2 bulk at 115°C (e) splits up into four peaks: the parameters of the fit of peaks 2 and 3 are indicated on the Figure; peaks 1 and 4 (black dashed lines) are purely Gaussian, with a_1 and a_4 being equal to 8.75×10^{-9} and 2.03×10^{-9}, respectively; the other parameters are $I_1 = 6.05 \times 10^{-4}$, $q_1 = 0.107$ Å^{-1}, $\xi_1 = 1022$ Å and $I_4 = 7.69 \times 10^{-4}$, $q_4 = 0.116$ Å^{-1}, $\xi_4 = 1474$ Å, for peaks 1 and 4, respectively.

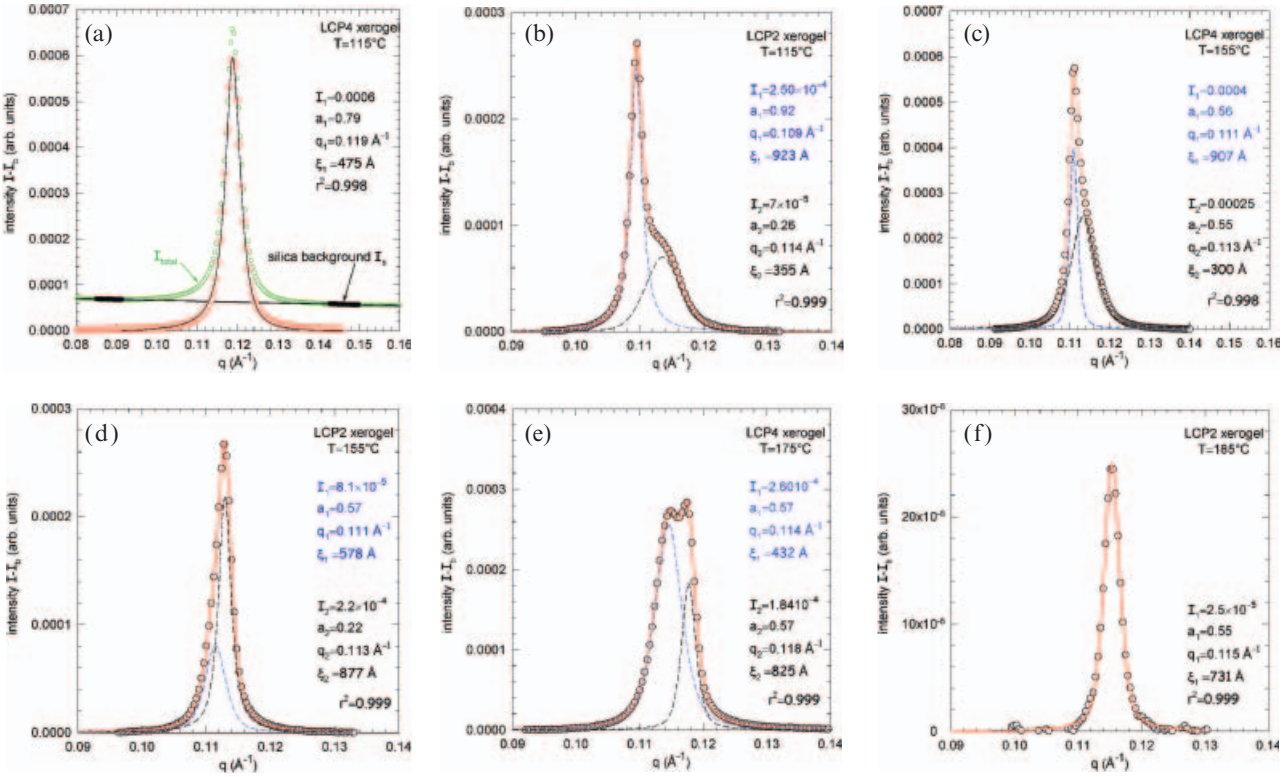

Figure 9. Examples of peak fitting in the case of LCP–xerogel nanocomposites. For all curves, the silica scattering background was subtracted as shown in (a).

scattering coming from the polymer backbone. The presence of iso-intensity points (Figure 6) would indicate that this background scattering is strongly related to the position and the shape of the diffraction peaks, i.e. to the smectic structure. At higher temperatures (170°C), the SAXS curve (Figure 8(c)) displays two different features: (i) a broad peak resulting from scattering of liquid polymer (isotropic phase) and (ii) a low intensity fine peak; after subtraction of the liquid order background, it appears that the peak has similar characteristics to that of the peak measured at 155°C, except that the position is shifted to a larger q-value (0.119 $Å^{-1}$ instead of 0.113 $Å^{-1}$).

As already shown in Figure 4(a), the SAXS curve obtained for bulk LCP2 displays multiple peaks below 140°C. An example of peak separation is given on Figure 8(e). The peaks located at the lowest and the highest q-values are pure Gaussian. Interestingly, the main peak measured at 115°C and located at 0.110 $Å^{-1}$ is very similar to that measured at 140°C (Figure 8(f)), but for the latter the smectic domain size (ξ=1452 Å) is larger than for the former (ξ=770 Å). Thus, it is likely that LCP2 displays a coexistence of SmC and SmA phases between 115 and 140°C. This point will be discussed in section 3.5.

For the analysis of the peaks of LCPs confined in the silica xerogel, it is necessary to subtract the background coming from silica scattering, as indicated in Figure 9(a) for LCP4–xerogel (115°C). The resulting peak is very similar to that obtained for the bulk sample (Figure 8(a)), but the size of the organised domains is smaller (ξ=475 Å) than in the bulk sample (ξ=1676 Å). This feature probably results from the presence of a silica network in the solution during crystallisation by evaporation of the solvent, which limits the LCP growth. The effect of confinement shows itself, above 145°C (Figure 4(d)), in peak splitting. Separation into two peaks is shown in Figure 9(c). Splitting is observed up to the highest temperature investigated (185°C), but the distance between the maxima increases (Figure 9(e)). Comparison between the LCP2 bulk polymer and the LCP2–xerogel peaks at 115°C (Figures 8(e) and 9(b), respectively) indicates a less complex structure in the LCP grown in the presence of silica than without: the two Gaussian peaks no longer exist. The two peaks observed in bulk and in confined LCP2 as well as the ratio between their intensity (3.57 and 3.94) are quite similar. At 155°C, the position of the peaks is the same for LCP2 and LCP4 xerogels (Figures 9(c) and 9(d)). Unlike for LCP4 xerogel at 185°C, peak splitting in

LCP2 xerogel (Figure 9(f)) no longer exists: LCP2 confined in the largest pores is in the isotropic phase.

3.5. *Analysis and discussion of the structural data deduced from the fit*

Figure 10 shows the variation of the values of d deduced from the fitting parameter q_i by means of the Bragg relation

$$d_i = 2\pi/q_i \qquad (3)$$

for the bulk LCP2 (figure 10(a)), bulk LCP4 (Figure 10(b)), LCP2 and LCP4 confined in the silica xerogel (Figures 10(c) and 10(d), respectively). As expected from Figure 4, all samples display a similar feature: the value of d goes through a maximum d_M at a temperature T^* that depends on the sample. The values of d_M shown in Figure 10 are not exactly the same for the different samples. They range between 58.4 Å (bulk LCP2) and 57.0 Å (bulk LCP4). The uncertainty on d_M, estimated to be ± 0.2 Å, does not account for the difference. Meanwhile, near T^*, d_M is very sensitive to the temperature. Because measurements were performed using steps of 0.5°C, it is

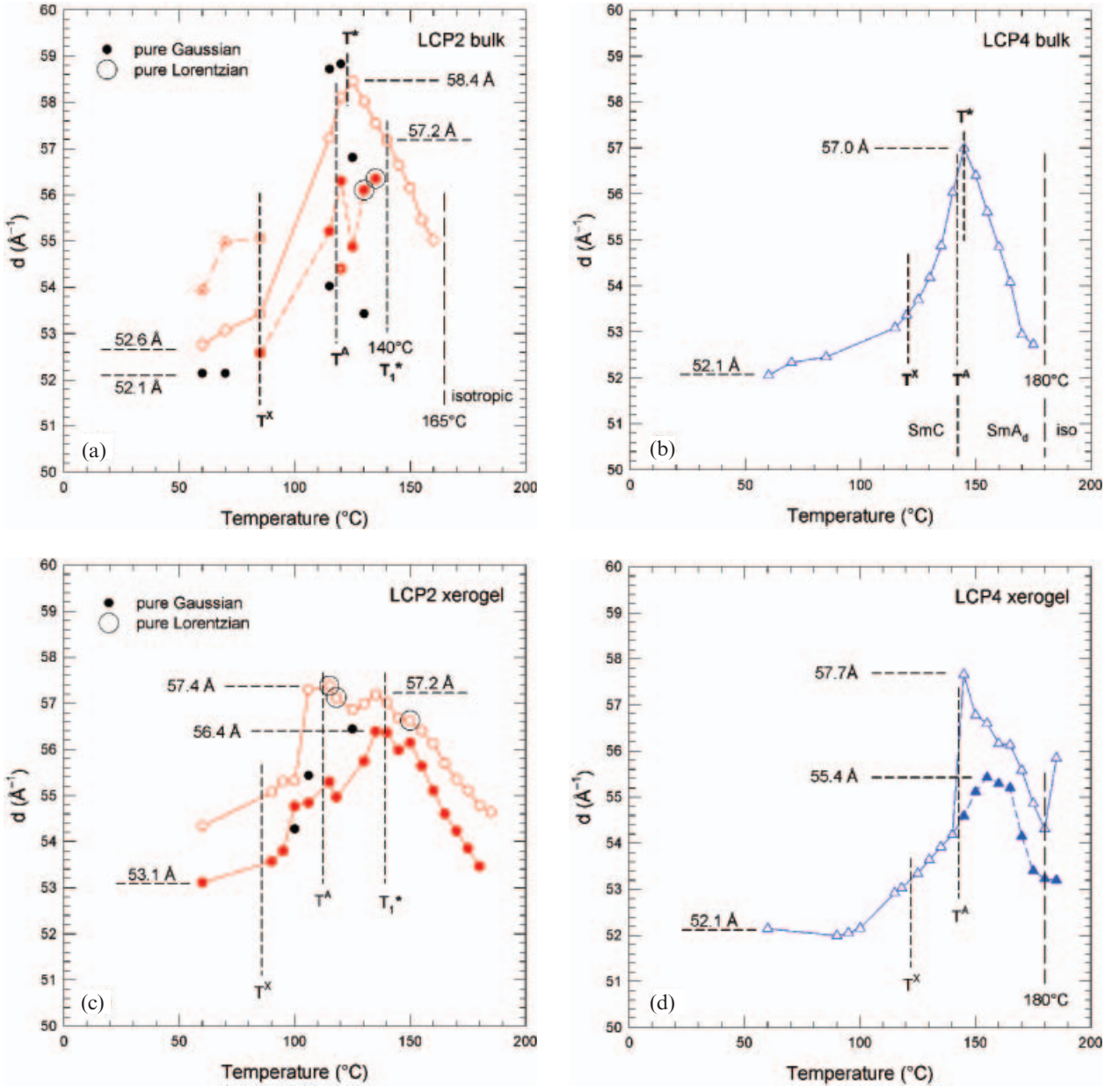

Figure 10. Variation with temperature of the inter-lamellar distances d obtained from the fit with pseudo-Voigt equations. The values of T^X, T^A, T^* and T_1^* indicated for the nanocomposites ((c) and (d)) are that obtained for the corresponding bulk sample.

possible that the real value of d_M is reached in this interval. It follows that the difference between 57.0 Å (bulk LCP4) and 57.7 Å (LCP4–xerogel) may have no physical meaning. As for bulk LCP2, there are two values of d, located on each side of T^*, which are larger than 57.7 Å. Thus, one may assume that the maximum lamellar d_M in LCP2 is slightly larger than in LCP4 and in LCP2–xerogel (Figure 10(c)).

POM textures (Figure 2) have shown that the ordering of these LCPs is SmC below T^*, and SmA above T^*. In the SmA mesophase, the side chains are perpendicular to the main chain. One may now compare the value of the lamellar spacing d_M determined experimentally to that of the calculated length l of the side chain in the SmA mesophase. Details of the calculation are given elsewhere (*41*). For the LCPs investigated here, l is equal to 34.2 Å. Comparison between l and d_M allows information about the local packing of the smectic layers. The ratio d_M/l is equal to 1.71 (with d_M=58.4 Å) for LCP2 and 1.67 (with d_M=57.0 Å) for LCP4. It follows that the degree of interdigitation ID, defined as

$$ID = 100\left(2 - \frac{d_M}{l}\right), \tag{4}$$

is equal to 29% and 33% for LCP2 and LCP4, respectively. This result agrees with that expected for SCLCP having a short spacer, as in the present case (four carbon atoms, Figure 1). In fact, the flexibility of the mesogenic moieties between the layers is not large enough to allow a great interdigitation and imposes a limit in the approach between the backbone chains. Such compounds form SmA_d mesophases (*42, 43*). In contrast, for SCLCP having a long spacer (11 carbon atoms) interdigitation is close to 100% (the SmA_1 mesophase) (*41*). For LCP2 and LCP4, the lengths of the interdigitated layers are equal to 10 and 11.4 Å, respectively. Since the length of the tail is equal to 12.5 Å, only the terminal tails are interdigitated, presenting a hydrophobic interaction. The d_M/l values (1.71 and 1.67, for LCP2 and LCP4, respectively) are similar because the spacer and chemical structures of the mesogenic group are the same. This observation confirms that the local packing of the layers and the interdigitation degree depend mainly on the chemical structure of the mesogenic group and on the number of carbon atoms in the spacer. The slight actual difference between the two values could stem from the difference in the number of side chains n in the backbone for LCP2 and LCP4. This observation suggests that the molecular weight also plays a role, yet probably secondary, in the local packing of the chains. As suggested by Yamaguchi and Asada (*44*), the mobility of the side chain attached near to the end of the main chain should be different from that of the side chain attached in the middle of the main chain. For LCP2, the number of side chains is equal to 18, while it is much larger (51) in LCP4. Thus, end effects are expected to play a more important role in the former than in the latter. Since higher side-chain mobility involves a weaker interaction between side chains, and between side chains and backbone, an increase of the lamellar distance can be expected, as is observed for LCP2.

As already mentioned, the mesophase is SmC at temperatures below T^*. In this way, the increase of the layer thickness observed in Figure 10(b) for the bulk LCP4 between 60 and 145°C is due to the tilt of the mesogenic lateral groups to the normal of the layers in the SmC mesophase, which becomes zero in the SmA phase The temperature range for the SmC mesophase (up to T^*) is very similar to that observed using POM and by DSC (Figure 3) yielding T^A=144°C for the SmC–SmA transition on heating LCP4. It follows that T^* and T^A can be considered as equal. The minimum d values ($d_{min}=d_{SmC}$) range between 52.1 and 52.6 Å for the bulk LCP4 and LCP2, respectively. The interdigitation degree between the mesogenic groups depends on the chemical structure. Thus we have to consider that in the bulk polymers the interdigitation degree between the side chains in the SmC phase is the same in the SmA phase, the only difference being the tilt angle. The tilt angle in SmC can be determined by means of the following relation:

$$\theta = \cos^{-1}(d_{SmC}/d_{SmA}) \tag{5}$$

where $d_{SmA}=d_M$. Using d_{SmA}=58.4 Å and 57.0 Å for LCP2 and LCP4, respectively, and the above values of SmC, the imposed tilt angles of the mesogenic groups to the normal of the layer in each case are 23.9° and 25.7° for the bulk LCP4 (below 100°C) and LCP2 (below 85°C), respectively. Above these temperatures, d begins to increase, as a result of the decrease of θ to zero at T^*. Figure 10(b) indicates that the SmC–SmA transition extends over about 20°C for LCP4. Similar features have been observed for a low molecular weight LC (TBBA) (*45*) and more recently for liquid crystalline amphiphilic di-block copolymers (*33*). By contrast, the SmC^*–SmA transition in a low molecular weight ferroelectric LC appears as a critical phenomenon occurring within a domain of 0.1°C (*46*).

For bulk LCP2, the complexity of the SAXS curves (Figures 4(a) and 8(e)) up to T_1^*=140°C suggests a mixture of SmC phases characterised by different lamellar spacings (or tilt angles).

Interestingly, a unique SmA phase is observed for LCP2 above T_1* which is very close to T* observed for LCP4.

DSC measurements have indicated the presence of an endothermic effect at a temperature T^X indicated by a dashed line in Figures 10(a) and (b). For LCP4 (Figure 10(b)), T^X clearly corresponds to the temperature above which the interlayer distance d increases strongly with temperature. For LCP2, the lack of experimental data between 85 and 115°C does not allow a definite statement but only a realistic assumption of the relation between the thermal effect and the increase of d. Similar features have been reported by Watanabe et al. (*33*) for LC amphiphilic di-block copolymers. These authors attributed the thermal event to a transition between an unknown smectic phase (SmX) and SmC. In the case of TBBA, Guillon and Skoulios (*45*) have shown the existence of a smectic B phase between the crystal and the smectic C phases. The experimental results obtained for the present LCP samples do not permit one to characterise precisely the nature of this intermediate mesophase.

Considering now the LCP4–xerogel nanocomposite (Figure 10(d)), the splitting into two peaks observed at T* (=145°C) yields two different d_M values: 57.7 and 55.4 Å. The first one, as already discussed, can be considered as similar to that observed for bulk LCP. The second one is smaller. This feature could be attributed to the existence of two populations of pores in the silica xerogel, expected in a sol-gel reaction. A first series of pores would be large enough to allow the normal SmC–SmA transformation. In smaller pores, as a result of the large volume expansion involved in this transformation, there may not be enough space for the SmA phase to be formed. In this condition, confining LCP would either allow the SmC phase to remain up to higher temperature or the SmA phase to be formed providing a partial folding of the non-rigid terminal chain.

In the case of the LCP2–xerogel nanocomposite (Figure 10(c)), the number, the position and the temperature dependence of the peaks are also modified by confinement. As a matter of fact, bulk LCP2 (Figure 10(a)) shows a single phase SmA_d when T becomes larger than 135°C. For LCP2–xerogel, one observes the coexistence of different SmC phases below 135°C. This effect probably also results from the low molecular weight (*44*) of LCP2, as discussed above. Comparison between Figures 9(a) and 9(c) indicates the coexistence of mainly two different SmC or SmA phases over the whole range of temperature in LCP2–xerogel. Above 135°C, the origin of this effect is probably the same as for the LCP4–xerogel. Meanwhile, a precise comparison between the two LCP–xerogels is actually not possible. The silica porosity formed in the presence of LCP in solution could not be the same, despite the same experimental conditions, as a result of a possible influence of the molar mass difference between LCP2 and LCP4 on the gel formation. Also, owing to the fact that none of the LCPs became isotropic at 185°C (the maximum temperature experimentally available), the mesoporous structure of the silica grown in the presence of LCP could not be investigated in the LCP–xerogels.

Figure 10 also shows that, for all samples, d decreases above T*. A decrease of the interlayer spacing in interdigitated SmA structure has been observed by several authors (*17, 47*). Richardson and Herring (*17*) assume that an interdigitated structure is sensitive to the chain mobility. Meanwhile, in the present case, the side chains are weakly interdigitated. An explanation for the decrease of d could be the effect of the long tail that might tend to spread out (*48, 49*) in such a way that the mesogenic side chain would no longer be fully extended at higher temperature and become shorter. This effect would induce the decrease of the SmA interlayer distance. Such an explanation would also be consistent with the observation of iso-intensity points (Figure 6), which are assumed to stem from a link between interlayer and polymer backbone structure.

Figure 11 shows that, for bulk LCP4, the smectic domain size ξ, related to the number of smectic

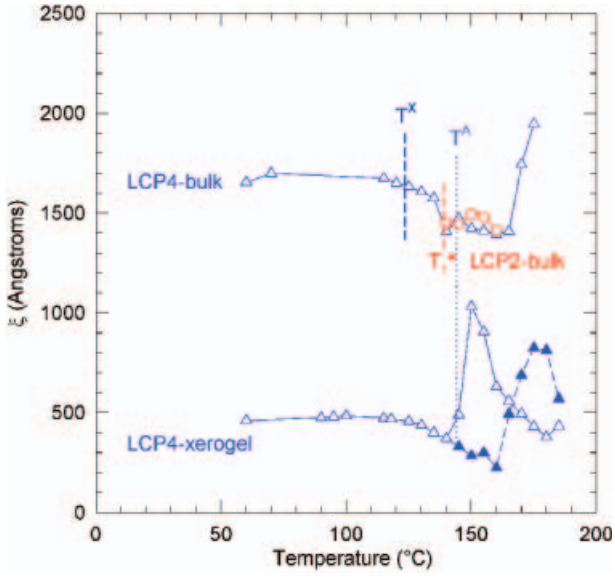

Figure 11. Variation of the smectic domain size of the ordered domains as a function of temperature for bulk and confined LCP4. The values of ξ obtained for bulk LCP2 above 140°C (single configuration) are shown by open circles.

layers, decreases slightly between T^X and T^A. This result suggests that the volume increase with temperature in the SmC phase is accompanied by some deterioration of the smectic arrangement. In the SmA phase, ξ remains constant up to 165°C, despite the decrease of the interlayer spacing. For LCP4–xerogel, ξ is significantly smaller. This result is consistent with crystallisation in a confined medium, during the sol-gel-drying process. Between T^X and T^A, ξ slightly decreases as in bulk LCP4. Interestingly, at the SmC–SmA transition temperature T^A ($=T^*$), the value of ξ corresponding to the SmA structure also jumps. This observation suggests a local reorganisation of the smectic layers in the large pores. Figure 11 also shows that ξ is nearly the same for LCP4 and LCP2 bulk, above T_1^*, i.e. when the latter displays a unique SmA structure. It should be noted also that the interlayer spacings are also the same between T_1^* and the isotropisation temperature T_i=165°C for LCP2 bulk.

In order to strengthen the above results deduced from the fit with one or more pseudo-Voigt equations and to go one step further in the analysis of the data, we have investigated the behaviour, with temperature, of the area Q of the fundamental peak (peak 1) and of the ratio I_2/I_1 between the intensity of the first harmonic (peak 2) and that of peak 1. The variation of the area Q of the peak (obtained by radial averaging over 2π), determined by graphical integration,

$$Q = \sum I(q)q^2\Delta q, \qquad (6)$$

is plotted in Figure 12(a), for bulk LCP2 and LCP4. For LCP4, Q slightly decreases between T^X and T^A (T^*). This decrease is consistent with the diminution of ξ, i.e. a diminution of the number of smectic layers. Above 160°C, the strong decrease of Q associated with constant (or increasing) values of ξ can be attributed to the diminution of the number of smectic domains in the illuminated volume as a result of partial melting. This explanation is consistent with the disappearance of the iso-intensity points above 160°C shown in section 3.3. This result indicates a two phase region (SmA and isotropic) above 160°C as also found by other authors (*17, 48*) and confirmed by the POM picture shown in Figure 12 (insert). Moreover, the increase of ξ in this temperature range suggests a rearrangement of the smectic layers owing to a larger available space. As mentioned in section 3.4, the ratio I_2/I_1 is related to the rigidity of the smectic layers. The strong decrease of I_2/I_1 around T^X for LCP4 (Figure 12(b)) reveals larger thermal fluctuations above this temperature. This feature reinforces the previous explanation about the origin of the thermal effect occurring at T^X. The corresponding transition would occur between two smectic phases characterised by a different rigidity of the smectic layers. Above T^X, thermal fluctuations in the SmC phase would allow the decrease of the tilt angle to zero at T^A (T^*). For LCP4 confined in the silica xerogel and for bulk LCP2 above T_1^* (single peak), the values of I_2/I_1 are very similar to those obtained for bulk LCP4. It follows that the characteristics of the smectic A layers itself are almost independent of the molecular weight. For the sol-gel confined LCP4,

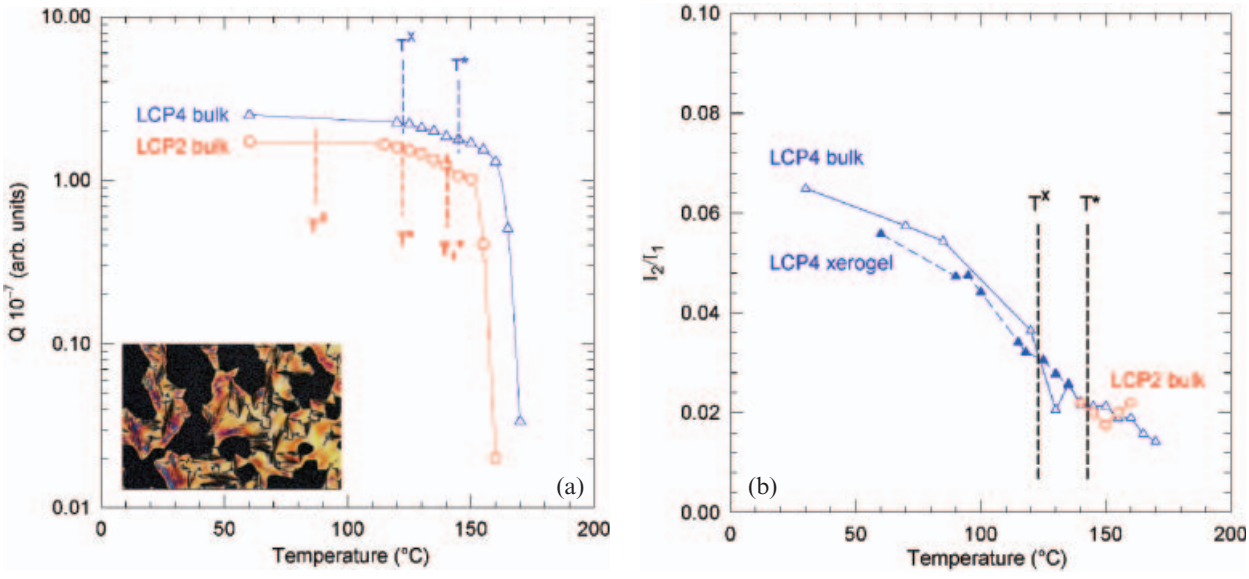

Figure 12. Variation with temperature of the peak area Q (a) and of the ratio I_2/I_1, for bulk LCP2 and LCP4. The insert in (a) shows the POM image of LCP4 at 170°C.

the SmC layers are similar to that achieved in the bulk; as for the SmA layers, this observation is also valid for the fraction of LCP located in pores large enough to allow the dilatation related to the SmC–SmA transition. The above comments suggest that the lowering of the isotropisation temperature T_I with the molecular weight or its increase for the sol-gel confined samples cannot be related to a modification of the layer rigidity. It is likely that T_I is mainly affected by the lateral size of the layers or by a stabilising interaction with silica.

4. Conclusion

The mesophase behaviour of a side-chain liquid crystalline polyacrylate grown by drying a solution was investigated. This LCP had a short spacer (four carbon atoms) and a long tail (10 carbon atoms). The parameters involved in this study were the mean molecular weight of the LCP, i.e. the mean number of side chains per polyacrylate main chain, and confinement in the case of LCP–silica nanocomposites prepared by a sol-gel process. The LCP, having 18 side chains (LCP2), is characterised, in bulk, by a mixture of domains having different lamellae widths and probably also, in a given range of temperatures, by the coexistence of SmC and SmA phases. Increasing the number of side chains up to 51 allows well-defined single phases to be formed. Coexistence of two phases is only observed near the isotropisation temperature, where SmA phases are still present in the isotropic melt.

For the sol-gel LCP–silica nanocomposites, the isotropisation temperature T_I is larger than for the bulk LCP. Furthermore, the SmC–SmA transition that involves an expansion of the lamellar width, and, therefore, of the LCP volume, is modified by confinement. A behaviour similar to that of the bulk LCP is only possible in larger pores. The mesophase behaviour of these samples after heating above T_I (second heating), for which the LC ordering grows in the melt, as well as the effect on a magnetic field, will be reported in a forthcoming paper.

Acknowledgments

The authors are grateful to the CAPES/COFECUB 411-03 program for financial support and to the ESRF, Grenoble, for access to the French CRG beamline D2AM. They also acknowledge the help of its technical staff, J.F. Berar, N. Boudet, B. Caillot and S. Arnaud. They also thank P. Gonçalves for the theoretical calculations, C. Kloster and A. Rigacci for their help in the preparation of silica–LCP nanocomposites, L.F. Schelp for his participation in the SAXS measurements and stimulating discussions, and I. Grillo for her help in the curve fitting by means of the NLR equation.

References

(1) Wendorff J.H.; Finkelmann H.; Ringsdorf H. *J. Polym. Sci.: Polym. Symp*. **1978,** *63*, 245–261.
(2) Donald A.; Windle A.; Hanna S. *Liquid Crystalline Polymers;* Cambridge University Press: Cambridge, 2006 (and references therein).
(3) Shilov S.V.; Skupin H.; Kremer F.; Gebhard E.; Zentel R. *Liq. Cryst*. **1997,** *22*, 203–210.
(4) Brehmer M.; Zentel R.; Giesselmann F.; Germer R.; Zugenmaier P. *Liq. Cryst*. **1996,** *21*, 589–596.
(5) Whitcombe M.J.; Gilbert A.; Mitchell G.R. *J. Polym. Sci. Pol. Chem*. **1992,** *30*, 1681–1691.
(6) Symons A.J.; Davis F.J.; Mitchell G.R. *Polymer* **1999,** *40*, 5365–5370.
(7) Hessel F.; Finkelmann H. *Makromolekulare Chemie-Macromol. Chem. Phys*. **1988,** *189*, 2278–2283.
(8) Voigtmarting I.G.; Durst H.; Reck B.; Ringsdorf H. *Macromolecules* **1988,** *21*, 1620–1626.
(9) Davidson P.; Levelut A.M. *Liq. Cryst*. **1992,** *11*, 469–517.
(10) Davidson P. *Struct. Bond*. **1999,** *95*, 1–39.
(11) Meyer R.B. *Mol. Cryst. Liq. Cryst*. **1977,** *40*, 33–48.
(12) Shibaev V.P.; Kozlovsky M.; Beresnev L.; Blinov L.; Platé N. *Polym. Bull*. **1984,** *12*, 299–301.
(13) Hsu C.S. *Prog. Polym. Sci*. **1997,** *22*, 829–871.
(14) Ebbutt J.; Richardson R.M.; Blackmore J.; McDonnell D.G.; Verrall M. *Mol. Cryst. Liq. Cryst*. **1995,** *261*, 549–566.
(15) Basu S.; Rawas A.; Sutherland H.H. *Mol. Cryst. Liq. Cryst*. **1986,** *132*, 23–28.
(16) Del Campo A.; Bello A.; Perez E. *Macromol. Chem. Phys*. **2003,** *204*, 682–691.
(17) Richardson R.M.; Herring N.J. *Mol. Cryst. Liq. Cryst*. **1985,** *123*, 143–158.
(18) Galli G.; Chiellini E.; Laus M.; Angeloni A.S.; Francescangeli O.; Yang B. *Macromolecules* **1994,** *27*, 303–305.
(19) Ostrovskii B.I.; Sulyanov S.N.; Boiko N.I.; Shibaev V.P.; de Jeu W.H. *Eur. Phys. J. E* **2001,** *6*, 277–285.
(20) Merlo A.A.; Magnago R.V.; Vollmer A.F.; Mauler R.S.; Pereira F.V.; da Silveira N.P. *Polym. Bull*. **1999,** *42*, 551–557.
(21) Merlo A.A.; Ritter O.M.; Pereira F.V.; da Silveira N.P. *J. Braz. Chem. Soc*. **2001,** *12*, 184–191.
(22) Ritter O.M.S.; Merlo A.A.; Pereira F.V.; Geissler E.; Zukerman-Schpector J. *Liq. Cryst*. **2002,** *29*, 1187–1200.
(23) Vaia R.A.; Giannelis E.P. *Polymer* **2001,** *42*, 1281–1285.
(24) Huang W.; Han C.D. *Polymer* **2006,** *47*, 4400–4410.
(25) Huang W.; Han C.D. *Macromolecules* **2006,** *39*, 257–267.
(26) Ho C.Y.; Lee J.Y. *J. Appl. Polym. Sci*. **2006,** *100,* 1688–1704.
(27) Crawford G.P.; Žumer S. *Liquid Crystals in Complex Geometries Formed by Polymer and Porous Networks*; Taylor & Francis: London, 1996.
(28) Shojaei-Zadeh S.; Anna S.L. *Langmuir* **2006,** *22*, 9986–9993.
(29) da Silveira N.P.; Pereira F.V.; Rigacci A.; Ehrburger-Dolle F. *J. Therm. Anal. Calorim.* **2005,** *79*, 579–585.
(30) Pajonk G.M.; Elaloui E.; Achard P.; Chevalier B.; Chevalier J.-L.; Durant M. *J. Non-Cryst. Solids* **1995,** *186*, 1–7.

(31) Huang T.C.; Toraya H.; Blanton T.N.; Wu Y. *J. Appl. Cryst*. **1993,** *26*, 180–184.
(32) Collings P.J.; Hird M. *Introduction to Liquid Crystals Chemistry and Physics*; Taylor & Francis: London, 1997.
(33) Watanabe R.; Iyoda T.; Yamada T.; Yoshida H. *J. Therm. Anal. Cal*. **2006,** *85*, 713–717.
(34) Bahr Ch.; Heppke G. *Mol. Cryst. Liq. Cryst*. **1987,** *150b*, 313–324.
(35) Marzec M.; Popczyk J.; Fafara A.; Wrobel S.; Dabrowski R. *Ferroelectrics* **2002,** *281*, 123–134.
(36) Mukherjee P.K.; Deutsch M. *J. Chem. Phys*. **1999,** *110*, 2680–2683.
(37) Rappaport A.G.; Clark N.A.; Thomas B.N.; Bellini T. X-ray Scattering as a Probe of Smectic A Liquid Crystal Ordering in Silica Aerogels. In *Liquid Crystals in Complex Geometries*; Crawford G.P., Zumer S. (Eds), Taylor & Francis: London, 1996; pp. 411–466.
(38) Dewettinck K.; Foubert I.; Basiura M.; Goderis B. *Cryst. Growth Des*. **2004,** *4*, 1295–1302.
(39) Nallet F.; Laversanne R.; Roux D. *J. Physique II* **1993,** *3*, 487–502.
(40) Leheny R.L.; Park S.; Birgeneau R.J.; Gallani J.-L.; Garland C.W.; Iannacchione G.S. *Phys. Rev. E* **2003,** *67*, 011708–1–13.
(41) Pereira F.V.; Borsali R.; Ritter O.M.S.; Gonçalves P.F.; Merlo A.A.; Silveira N.P. *J. Braz. Chem. Soc*. **2006,** *17*, 333–341.
(42) Hardouin F.; Sigaud G.; Keller P.; Richard H.; Nguyen Huu Tinh; Mauzac M.; Achard M.F. *Liq. Cryst*. **1989,** *5*, 463–478.
(43) Demus D.J.; Goodby G.W.; Gray H.-W.; Spiess V.V. *Handbook of Liquid Crystals*; Wiley-VCH: Weinheim, 1997.
(44) Yamaguchi T.; Asada T. *Liq. Cryst*. **1991,** *10*, 215–228.
(45) Guillon D.; Skoulios A. *J. Physique* **1997,** *38*, 79–83.
(46) Ratna B.R.; Shashidhar R.; Nair G.G.; Prasad S.K.; Bahr Ch.; Heppke G. *Phys. Rev. A* **1988,** *37*, 1824–1826.
(47) Soltysiak J.T.; Bialecka-Flojanczyk E.; Przedmojski J. *Eur. Polym. J*. **2006,** *42*, 1662–1669.
(48) Auad M.L.; Kempe M.D.; Kornfield J.A.; Rendon S.; Burghardt W.R.; Yoon K. *Macromolecules* **2005,** *38*, 6946–6953.